Mathematical Biosciences 359 (2023) 108997

Contents lists available at ScienceDirect

Mathematical Biosciences

journal homepage: www.elsevier.com/locate/mbs

Original Research Article

A multiscale hybrid model for exploring the effect of Resolvin D1 on macrophage polarization during acute inflammation

Jeroen F. Uleman [a,b,c,*], Emiliano Mancini [b,d,e], Rushd F.M. Al-Shama [f], Anje A. te Velde [b,g], Aletta D. Kraneveld [h], Filippo Castiglione [b,i,j]

[a] Department of Geriatric Medicine, Radboudumc Alzheimer Center, Donders Institute for Medical Neuroscience, Radboud University Medical Center, Geert Grooteplein Zuid 10, 6500HB, Nijmegen, The Netherlands
[b] Institute for Advanced Study, Amsterdam, The Netherlands
[c] Section of Epidemiology, Department of Public Health, University of Copenhagen, Copenhagen, Denmark
[d] Data Science Institute, Hasselt University, Hasselt, Belgium
[e] Department of Global Health, Amsterdam UMC, Amsterdam, The Netherlands
[f] Department of Clinical and Experimental Cardiology, Amsterdam Cardiovascular Sciences, Amsterdam UMC, University of Amsterdam, Heart Center, Amsterdam, The Netherlands
[g] Tytgat Institute for Liver and Intestinal Research, AGEM, Amsterdam UMC, University of Amsterdam, Amsterdam, The Netherlands
[h] Division of Pharmacology, Utrecht Institute for Pharmaceutical Sciences, Faculty of Science, Utrecht University, The Netherlands
[i] Institute for Applied Computing, National Research Council of Italy, Rome, Italy
[j] Biotech Research Center, Technology Innovation Institute, Masdar City, Abu Dhabi, United Arab Emirates

ARTICLE INFO

Keywords:
Multiscale model
Resolvin D1
Acute inflammation
Agent-based model
Gene-regulatory network
Macrophage polarization

ABSTRACT

Dysregulated inflammation underlies various diseases. Specialized pro-resolving mediators (SPMs) like Resolvin D1 (RvD1) have been shown to resolve inflammation and halt disease progression. Macrophages, key immune cells that drive inflammation, respond to the presence of RvD1 by polarizing to an anti-inflammatory type (M_2). However, RvD1's mechanisms, roles, and utility are not fully understood.

This paper introduces a gene-regulatory network (GRN) model that contains pathways for RvD1 and other SPMs and proinflammatory molecules like lipopolysaccharides. We couple this GRN model to a partial differential equation–agent-based hybrid model using a multiscale framework to simulate an acute inflammatory response with and without the presence of RvD1. We calibrate and validate the model using experimental data from two animal models.

The model reproduces the dynamics of key immune components and the effects of RvD1 during acute inflammation. Our results suggest RvD1 can drive macrophage polarization through the G protein-coupled receptor 32 (GRP32) pathway. The presence of RvD1 leads to an earlier and increased M_2 polarization, reduced neutrophil recruitment, and faster apoptotic neutrophil clearance.

These results support a body of literature that suggests that RvD1 is a promising candidate for promoting the resolution of acute inflammation. We conclude that once calibrated and validated on human data, the model can identify critical sources of uncertainty, which could be further elucidated in biological experiments and assessed for clinical use.

1. Introduction

Dysregulated resolution of inflammation underlies the development and progression of various chronic and acute diseases. Lifestyle interventions related to sleep [1], physical exercise [2], and diet [3] have been proposed to reduce inflammation. Omega-3 polyunsaturated fatty acids (PUFAs), specifically eicosapentaenoic acid and docosahexaenoic acid (DHA) are dietary supplements that have favorable effects on cardiovascular outcomes [4,5]. PUFAs are naturally present in fish and spices such as turmeric [6].

One PUFA metabolite of particular interest is Resolvin D1 (RvD1). RvD1 is a specialized pro-resolution lipid mediator (SPM) derived from DHA that shows potent anti-inflammatory effects in several animal

Abbreviations: RvD1, Resolvin D1; GRN, Gene-regulatory network; ABM, Agent-based model; PUFA, Polyunsaturated fatty acid; SPM, Specialized pro-resolution lipid mediator; PDE, Partial differential equation

* Corresponding author at: Section of Epidemiology, Department of Public Health, University of Copenhagen, Øster Farimagsgade 5, 1353, Copenhagen K, Denmark
E-mail address: jeroen.uleman@sund.ku.dk (J.F. Uleman).

https://doi.org/10.1016/j.mbs.2023.108997
Received 22 October 2022; Received in revised form 23 March 2023; Accepted 24 March 2023
Available online 29 March 2023

models of inflammation, including acute lung injury [7], renal injury in heart failure [8], and sepsis-induced cardiac injury [9]. Additionally, the protective role of RvD1 extends to adverse tissue remodeling. In a mouse model of aortic dissection, RvD1 prevented aortic disintegration and increased the survival rate of treated versus untreated rats [10], illustrating its ability to resolve inflammation and halt fibrotic processes. These studies report that RvD1 administration attenuated the infiltration of inflammatory macrophages.

Macrophages are phagocytic leukocytes that are ubiquitously present and have remarkable plasticity that allows them to respond to environmental cues. Aberrant macrophage responses contribute to the pathogenesis of chronic inflammatory diseases [11,12]. SPMs like RvD1 can promote the resolution of inflammation by stimulating these activated cells to undergo a phenotypic switch from a pro- (M_1) to an anti-inflammatory (M_2) phenotype [13].

While pre-clinical data have shown promising results, clinical trials have yielded conflicting results. For example, even though RvD1 prevented atrial fibrillation-promoting electrical and structural remodeling in a rat model of right heart disease, omega-3 supplementation appears to increase the risk for atrial fibrillation in humans [14]. Furthermore, PUFA supplementation after myocardial infarction was associated with a lower risk of major cardiovascular events but a higher risk for atrial fibrillation onset [15]. These complex effects suggest that a deeper mechanistic understanding of specific SPMs is necessary for their utility in clinical practice. Computational models can be used to this end.

Computational modeling can complement experimental studies by addressing questions that either cost too much time or money or cannot be studied using in vitro experiments [16,17]. Computational models may suggest new hypotheses and support or disprove previously formulated ones [18]. Multiscale models are particularly promising as they transcend space–time scales of biological organization and, in some instances, embed microscopic mechanisms into mesoscopic- or macroscopic-level descriptions [19]. In Appendix A, we provide a quick panoramic view of the computational methods used to model the phenomena of immune system inflammation. In this paper, we describe the development of a multiscale model for studying the effects of RvD1 on macrophage differentiation in the resolution of acute inflammation.

2. Materials and methods

Our multiscale model simulates a portion of acutely inflamed tissue containing white blood cells and several molecules involved in the inflammatory process. It consists of three sub-models. Firstly, an agent-based model describes the dynamics of macrophages, neutrophils, and T-helper lymphocytes. Secondly, a partial differential equation model describes the kinetics of the concentration of pro- and anti-inflammatory cytokines, one chemokine, and RvD1 over space and time. These two coupled models describe the extracellular dynamics of an innate immune response to an antigen, together with the recruitment of immune cells into the simulated space. Finally, a gene-regulatory network model represents the main genes involved in the differentiation/polarization of macrophages and determines how they respond to stimuli from other cell types. The role of the gene-regulatory network is to represent the intracellular mechanisms triggered within the macrophages that lead to the expression of different genes in response to the state of the extracellular space around each cell. Specifically, the triggers we account for in this model are the concentration of various cytokines in the same grid point occupied by a specific macrophage, the antigen concentration, and the cell–cell interactions that drive the innate immune response. The coupling of these three models at two levels of description (intra- and extracellular) allows for insights into how RvD1 affects the acute inflammatory response through macrophage differentiation. In Sections 2.1–2.2, we provide a mathematical description for these sub-models before describing how the multiscale model was calibrated and validated in Section 2.3 and detailing the simulation experiment we conducted involving RvD1 in Section 2.4.

2.1. Gene-regulatory network model

We started by extending a previously developed Boolean gene-regulatory network (GRN) model based on a network by Castiglione et al. [20], which described a network of 18 nodes representing extracellular stimuli, membrane receptors, intracellular transducers, transcription factors, and target genes in a macrophage. The configuration of nodes in this undirected graph determines whether a cell will be polarized to the proinflammatory M_1 or anti-inflammatory M_2. We conducted a literature review to extend the GRN by Castiglione et al. [20] with additional nodes that allow for modeling the effects of SPM. A description of the edges with corresponding references from the scientific literature is provided in Appendix B. The edges are either inhibitory or excitatory, which means that they repress or stimulate the activation, respectively. A schematic overview of the GRN model we developed is given in Fig. 1. Black arrows (edges) represent excitatory relationships among nodes, whereas red arrows represent inhibitions.

The network state is updated at each time step (t) given the adjacency matrix (Eq. (1)). This equation states that each node (x_i) is active *if and only if* it receives at least one excitatory signal (E_{i^+}) (i.e., at least one node with an excitatory edge impinging on x_i has an activation level equal to 1) and no inhibitory signals (E_i^-) at all (i.e., none of the nodes that have an inhibitory edge to x_i has an activation level of 1). At each time step, all nodes are updated simultaneously so that the value of a node at time $t+1$ only depends on the value of the nodes that impinge upon it at time t.

$$\begin{aligned} &\forall i = 1, \dots, N \\ &x_i^{t+1} = F\left(x_i^t, \dots, x_N^t\right) \\ &\quad = \bigvee_{j \in E_i^+} x_j^t \wedge \neg \bigvee_{j \in E_i^-} x_j^t \end{aligned} \tag{1}$$

Stable states of the network dynamics define the polarization state of a cell [20]. A stable state is reached at time t' when $\forall t > t', \forall i \quad x_i(t) = x_i\left(t'\right)$. Theoretically, the system can also reach a limit cycle (i.e., a repeated sequence of states), but this GRN has only stable states [20]. While in general, t' can be very large (yet $t' < \infty$), in our case, it is relatively small, namely ten. Within ten update steps, a macrophage can thus progress to a differentiated (stable) state or not. If it does not, the macrophage polarization state is undefined and considered undifferentiated (M_0).

Macrophage polarization towards M_1 is defined as a stable state in which the activation of Arg1 gene is 0 and iNOS gene 1. Conversely, in a stable state where activation of Arg1 1 and iNOS is 0, the macrophage is defined to have polarized towards M_2. Polarization towards M_0 has been defined as any stable state where Arg1 and iNOS are both inactive, with an activation of 0. Due to mutual inhibition by their activating nodes, Arg1 and iNOS are never simultaneously active.

At every time step of the hybrid agent-based–partial differential equation model (Section 2.2), a GRN model is updated for each macrophage until a stable state of each GRN's dynamics is reached. The stable state reached depends on the concentration of the different molecules (corresponding to the input nodes in Fig. 1) in the grid point where the specific macrophage resides at that instant of time. If the concentration of a molecule is high enough, the corresponding input node will be activated.

The stable state that is ultimately reached is not affected by the initial activation state of the network (including the macrophage's previous polarization state) and thus solely depends on the activation of the input nodes. In this GRN model, IL4 and RvD1 have strong anti-inflammatory effects that inhibit the proinflammatory effects of the DLL4, IFNγ, and LPS. For instance, in the presence of high concentrations of IFNγ and LPS, the network reaches a stable configuration that we interpret as the M_1 polarization state of the macrophage, whereas a high concentration of IFNγ and LPS in the presence of RvD1 or IL4 would result in polarization to the M_2 phenotype. In contrast, IL10 inhibits only the proinflammatory effect of LPS but not DLL4 and IFNγ.

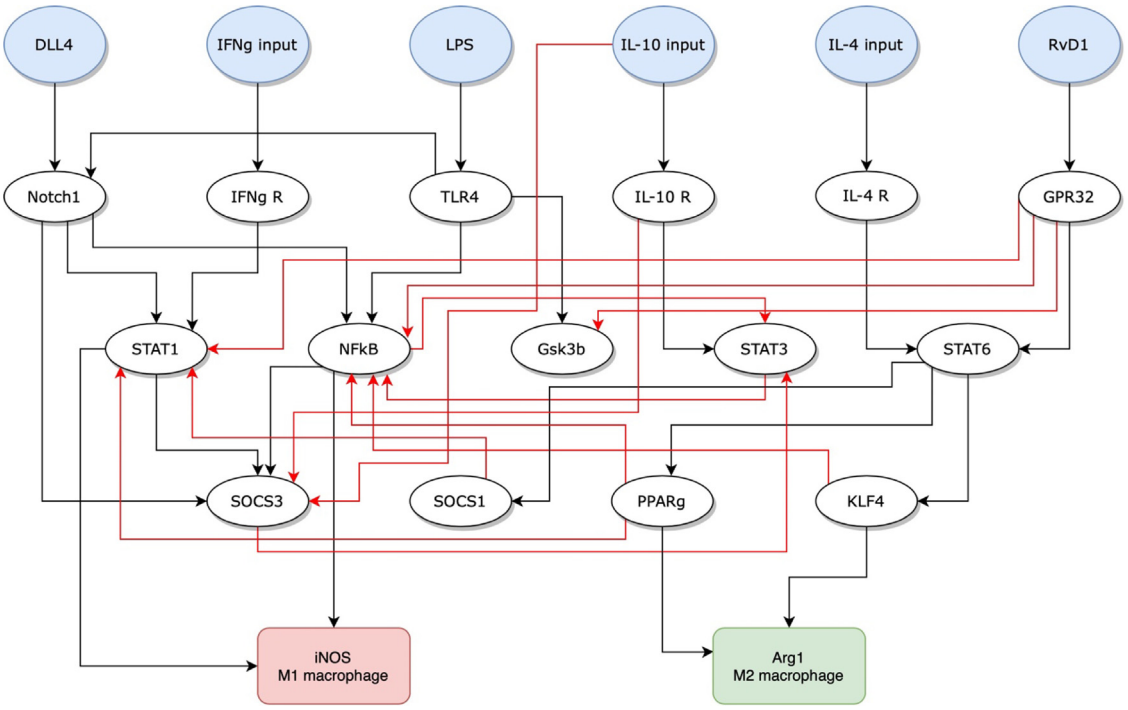

Fig. 1. The gene-regulatory network model of macrophage polarization. The blue nodes represent the inputs to external stimuli triggering the gene-regulation programs culminating in the polarization of the macrophage to an M_1 (red) or M_2 (green) state.

2.2. Hybrid agent-based–partial differential equation model

Besides a gene-regulatory network that determines the state of a macrophage, our model incorporates both an agent and an environment layer [21] at the tissue level. In particular, we utilize the agent-based modeling (ABM) paradigm to represent agents interacting at the tissue level (*agent layer)* coupled with a set of partial differential equations to describe the diffusion of molecules over a grid (*environment layer)*.

The hybrid model described in this manuscript leans on the earlier work by Su et al. [22], who developed an extensive partial differential equation (PDE) inflammatory response model to model acute and chronic inflammation over space and time. Su et al. [22] accounted for neutrophils (N), apoptotic neutrophils (ND), activated (MA) and resting macrophages (MR), immature and mature dendritic cells, and effector (T) and regulatory (T_R) T-cells. They also modeled a generic antigen and cytokines that T, T_R, and MA secreted. All these cells and molecules diffuse in a discretized space on one or two dimensions. Their model enables a chronic or acute infection simulation, defined by a source function for the antigen. While the model does not include potentially relevant factors like B cells, NK cells, and CB8 T-cells, it accounts for core immune processes such as antigen recognition, inter-cell communication, movement, and effector functions (i.e., activation vs. inhibition). As such, the detailed description of the inflammatory response in Su et al. [22] was used as a reference for constructing the multiscale hybrid model presented here. In addition, we incorporated stochastic, agent-based interactions between cells, diffusion of molecules by partial differential equations, and polarization of macrophages through the gene-regulation machinery of a gene-regulatory network model (GRN). Each of these model components is described below.

2.2.1. The environment layer

The different molecules incorporated in our model are provided in Table 1. In agreement with Su et al. [22], our model includes a chemo-attractant or generic chemokine (CH). Examples of chemokines are CCL5 and CXCL1, secreted by macrophages and attract T-cells and neutrophils [23]. Additionally, our model contains anti-inflammatory cytokines secreted by M_2 macrophages (CM), which prevent neutrophil recruitment. Our model also includes antigens which we call lipopolysaccharides (LPS) but yield an equivalent function. Importantly, our model introduces RvD1, diffused over the grid, and assumed to be exogenously introduced. We also include DLL4, activated through interactions between proximal macrophages, expressing DLL4 on their cell wall when activated [24].

Table 1
The different molecules in the model, their sources and sinks, and whether they have a pro- or anti-inflammatory effect. LPS = Lipopolysaccharides; IFNγ = Interferon gamma; IL10 = Interleukin 10; IL4 = Interleukin 4; CH = Chemokines; CM = Cytokine secreted by M_2 polarized macrophages.

Molecule	Source	Sink	Proinflammatory	Anti-inflammatory
LPS	–	N, M_1, M_2	Yes	No
IFNγ	T	–	Yes	No
IL10	T_R	–	No	Yes
IL4	T_R	–	No	Yes
CH	M_1, M_2, N	–	No	No
CM	M_2	–	No	Yes

We use the model to simulate a portion of tissue of 0.05 μl exposed to an exogenous insult consisting of a dose of LPS molecules at time 0 (t_0). This volume is subdivided into a 2-dimensional layer of 20-by-20 voxels. The lattice has a von Neumann neighborhood with periodic boundary conditions (toroidal boundaries) as we assume the lattice to be an open piece of tissue rather than a contained space such as a Petri dish. Neutrophils and undifferentiated macrophages are the only cellular entities that populate the space initially. No T-cells are present at time zero as their recruitment from the periphery is consequential in initiating the inflammatory state [22].

Cells are sensitive to the local concentration of specific molecules through their membrane receptors. In the same way, the activation/differentiation state of macrophages is triggered by membrane receptors that bind molecules in the surrounding. The binding occurrence is modeled as a Boolean event whose probability is a function of the local concentration of specific molecules. Thus, the activation of a receptor (i.e., the input) node of the GRN is modeled as a sigmoid or Hill

function [25] of the concentration x of the receptor–ligand molecule $P(1|\theta,x) = \left(1+(\theta/x)^n\right)^{-1}$, with $n = 4$, which was selected to obtain a steep activation curve, and threshold θ given in Table 2 for each molecule.

The PDEs describing the time evolution of LPS, IFNγ, IL10, and IL4 are given by Eqs. (2)–(7), respectively. In these equations, D_x is the diffusion coefficient of molecule x, μ_x is the degradation rate of molecule x, $\lambda_{x|y}$ is the uptake rate of molecule x by agent y, and β_x is the secretion rate of molecule x. The concentration of each molecule diffused over the grid is assessed at each time step. Initially, no cytokines are present in the simulated volume.

$$\frac{\partial \mathrm{LPS}}{\partial t} = \mathrm{D_{LPS}}\Delta\mathrm{LPS} - \mu_{\mathrm{LPS}}\mathrm{LPS} - \left(\lambda_{\mathrm{LPS|M_0}}\mathrm{M_0} + \lambda_{\mathrm{LPS|M_A}}\left(\mathrm{M_1}+\mathrm{M_2}\right) + \lambda_{\mathrm{LPS|N}}\mathrm{N}\right)\mathrm{LPS} \quad (2)$$

$$\frac{\partial \mathrm{IFN}\gamma}{\partial t} = \mathrm{D_{IFN_\gamma}}\Delta\mathrm{IFN}\gamma - \mu_{\mathrm{IFN_\gamma}}\mathrm{IFN}\gamma + \beta_{\mathrm{IFN\gamma|T}}\mathrm{T} \quad (3)$$

$$\frac{\partial \mathrm{IL10}}{\partial t} = \mathrm{D_{IL10}}\Delta\mathrm{IL10} - \mu_{\mathrm{IL10}}\mathrm{IL10} + \beta_{\mathrm{IL10|T_R}}\mathrm{T_R} \quad (4)$$

$$\frac{\partial \mathrm{IL4}}{\partial t} = \mathrm{D_{IL4}}\Delta\mathrm{IL4} - \mu_{\mathrm{IL4}}\mathrm{IL4} + \beta_{\mathrm{IL4|T_R}}\mathrm{T_R} \quad (5)$$

$$\frac{\partial \mathrm{CH}}{\partial t} = \mathrm{D_{CH}}\Delta\mathrm{CH} - \mu_{\mathrm{CH}}\mathrm{CH} + \left(\beta_{\mathrm{CH|MA}}\left(\mathrm{M_1}+\mathrm{M_2}\right) + \beta_{\mathrm{CH|N}}\mathrm{N}\right)\mathrm{LPS} \quad (6)$$

$$\frac{\partial \mathrm{RvD1}}{\partial t} = \mathrm{D_{RvD1}}\Delta\mathrm{RvD1} - \mu_{\mathrm{RvD1}}\mathrm{RvD1} \quad (7)$$

In these equations $\mathrm{D_{LPS}}\Delta\mathrm{LPS} = \mathrm{D_{LPS}}\nabla^2\mathrm{LPS} = \mathrm{D_{LPS}}\left[\frac{\partial^2\mathrm{LPS}}{\partial x^2}, \frac{\partial^2\mathrm{LPS}}{\partial y^2}\right]$, which is the two-dimensional heat equation for conventional Fick diffusion. The numerical PDE solver used is detailed in Appendix C. The rates of $\mathrm{M_1}$ and $\mathrm{M_2}$ macrophages are assumed to be the same, $\lambda_{\mathrm{A|MA}}$, where $\mathrm{M_A}$ stands for "active macrophage". The values of the parameters in these equations are reported in Table 2.

While we simulate the diffusion of cytokines in the environment layer, the agent layer simulates the movement of the cells included in our model: macrophages, T-cells, and neutrophils. Several parameters rule their movement: the diffusion coefficient of each type D_{cell}, the linear size of a voxel (i.e., lattice point) Δx, and the time step Δt. Δt equals 60 min of real life, and the Δx is 50 μm. Fig. 2 provides an overview of the dimensions of the grid.

Initially, in the absence of the chemokine CH, the agents follow a random walk over the grid. Without CH, the agents choose any possible direction with an equal probability: $\frac{(1-p*)}{4}$, where p^* is the probability of remaining in the same position in a time step (Δt). This probability was estimated numerically to minimize the difference between the theoretical mean square displacement: $\mathrm{MSD}_t = 2d\,D_{\mathrm{cell}}\cdot\frac{t}{\Delta x^2}$, and the simulated mean square displacement, which was calculated by averaging over a large number (N) of simulations:

$$\mathrm{MSD}_s(t,p) = \left\langle \left|x_n(t,p) - x_n(0,p)\right|^2 \right\rangle = (1/N)\cdot\sum_{n=1}^{N}\left|x_n(t,p) - x_n(0,p)\right|^2,$$

in which d is the number of physical dimensions (i.e., $d = 2$) and $x_n(t,p)$ is the position after t steps with probability p of not moving at each time step Δt. As such, p^* is calculated according to Eq. (8).

$$p^* = \min_p\left\{\left|\mathrm{MSD}_s(t,p) - \mathrm{MSD}_t\right|\right\} \quad (8)$$

The obtained values of p^* are cell-specific since the diffusion coefficients are generally different (Table 3). In the following, we use p^*_T to indicate the probability of T and T_R remaining still and p^*_{M} for each macrophage type. The PDEs in Su et al. [22] model the chemotaxis of cells through a convection equation. In our ABM, this drifted motion is modeled as a biased random walk by modifying the uniform distribution of the random walk with jump probabilities proportional to the concentration of the chemokine CH in the neighboring grid points (i.e., pseudo-chemotaxis). Formally, once a cell decides to move with probability 1-p^*, the probability of moving to one of its four neighbors is in $\{p_1, \ldots, p_4\}$, with $p_i = \frac{c_i}{\sum_{j=1..4} c_j}$, in which c_i is the concentration of CH in the neighbor i.

Table 2
Parameter values for the environment layer. All values from Su et al. [22] are scaled to minutes and are within biological range unless annotated by *, in which case the values are estimates.

Parameter	Value	Unit	Reference
Secretion parameters			
$\beta_{\mathrm{IL4\|T_R}}$	4.2×10^{-5}	pg cell^{-1} min^{-1}	[22]
$\beta_{\mathrm{IL10\|T_R}}$	4.2×10^{-5}	pg cell^{-1} min^{-1}	[22]
$\beta_{\mathrm{IFN\gamma\|T}}$	4.2×10^{-5}	pg cell^{-1} min^{-1}	[22]
$\beta_{\mathrm{CM\|MA}}$	2.1×10^{-3}	pg cell^{-1} min^{-1}	[22]
$\beta_{\mathrm{CH\|MA}}$	6.9×10^{-5}	pg cell^{-1} min^{-1}	[22]
$\beta_{\mathrm{CH\|N}}$	3.8×10^{-4}	pg cell^{-1} min^{-1}	[22]*
β_{RvD1}	1.85×10^{-4}	pm cell^{-1} min^{-1}	Estimate
Uptake parameters			
$\lambda_{\mathrm{A\|M0}}$	1.7×10^{-4}	pg cell^{-1} min^{-1}	[22]
$\lambda_{\mathrm{A\|M_A}}$	5.5×10^{-4}	pg cell^{-1} min^{-1}	[22]
$\lambda_{\mathrm{A\|N}}$	3.8×10^{-4}	pg cell^{-1} min^{-1}	[22]*
Diffusion coefficients			
D_{LPS}	5.0×10^{-3}	μm^2 min^{-1}	[22]
D_{CH}	60	μm^2 min^{-1}	[22]
D_{IL4}	6.4	μm^2 min^{-1}	[22]
D_{IL10}	6.4	μm^2 min^{-1}	[22]
$D_{\mathrm{IFN\gamma}}$	6.4	μm^2 min^{-1}	[22]
D_{RvD1}	6.4	μm^2 min^{-1}	Estimate
Degradation parameters			
μ_{LPS}	7.2×10^{-8}	min^{-1}	[22]*
μ_{IL4}	2.6×10^{-3}	min^{-1}	[22]
μ_{IL10}	2.6×10^{-3}	min^{-1}	[22]
$\mu_{\mathrm{IFN\gamma}}$	1.5×10^{-3}	min^{-1}	[22]
μ_{CH}	2.0×10^{-2}	min^{-1}	[22]*
μ_{RvD1}	3.0×10^{-4}	min^{-1}	Estimate
μ_{CM}	1.5×10^{-3}	min^{-1}	[22]
Threshold parameters			
θ_{LPS}	3.94×10^{-3}	pg μl^{-1}	Estimate
θ_{IL10}	3.32×10^{-3}	pg μl^{-1}	Estimate
θ_{IL4}	2.26×10^{-4}	pg μl^{-1}	Estimate
$\theta_{\mathrm{IFN\gamma}}$	1.78×10^{-1}	pg μl^{-1}	Estimate
θ_{RvD1}	6.00×10^{-3}	pg μl^{-1}	Estimate

The lattice contains $20\times20 = 400$ grid points. Since macrophages, T-cells, and neutrophils have approximate diameters of d_{M}, d_{T}, and d_{N} of 21, 10, and 12 μm, respectively [26], we can compute the *approximate* maximum number of cells that can be contained in one grid point. For instance, for macrophages: $\mathrm{N_{apg_a}} = (\Delta x)^3\cdot\left(\frac{1}{6}\pi\mathrm{d}_{\mathrm{M}}^3\right)^{-1}$. This means that $50^3\left(\frac{\pi}{6}\cdot21^3\right)^{-1} \simeq 25$ macrophages can be contained in one grid point, which is in line with Tong et al. [27].

Parameters such as secretion and death rates from Su et al. [22] were turned into probabilities per Δt according to Eq. (9), in which r indicates the rate. The resulting probabilities are found in Table 3, along with the other pertinent parameters.

$$p = 1 - e^{-r\Delta t} \quad (9)$$

At t_0, the model is initialized with 400 undifferentiated macrophages, 5000 neutrophils, and no T-cells at random locations throughout the grid. Consecutively, undifferentiated macrophages, neutrophils, and effector T-cells are recruited based on the number of available agents outside the boundary: $\mathrm{M0}_b$, N_b, T_b (Table 3). These parameters are based on white blood cell counts [28]. For every N_b, $\mathrm{M0}_b$, or T_b, a number between 0 and 1 is drawn, leading to recruitment (i.e., appearance on the boundary of the grid) if the number is lower than recruitment probabilities ζ_T, ζ_M, and ζ_N. Whether a particular type of cell should be recruited or not depends on threshold parameters ϵ_{N}, ϵ_{TR}, ϵ_{T}, and ϵ_{M0}. These parameters specify the condition for which the agents will be recruited and introduce a smoothing step between the agent-based and partial differential equation models. The neutrophils, N, are exclusively recruited if the total sum of CM is lower than ϵ_{N} (Eq. (11)). Effector T-cells (T) and undifferentiated macrophages (M_0)

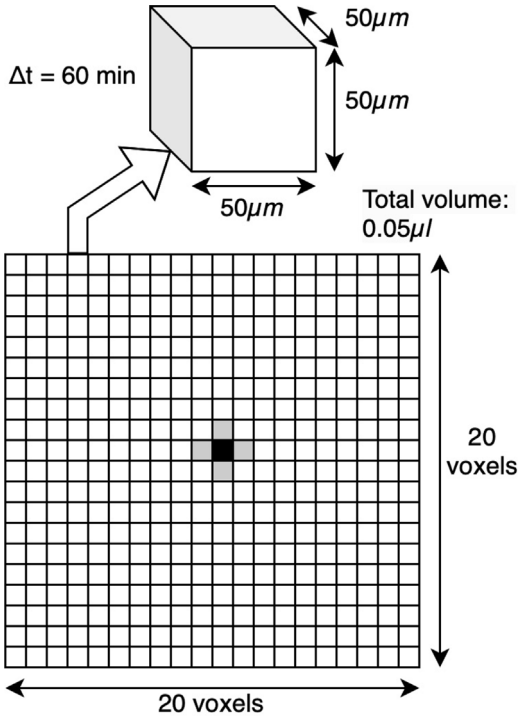

Fig. 2. Dimensions of the grid used in the agent-based and partial differential equation models. A single voxel dimension translates to 50 μm of actual space. At the center of the grid, the Von Neumann neighborhood is shown. The grid has periodic boundary conditions, which map the grid onto a torus.

are recruited as long as the integral of LPS is higher than ϵ_T and $\epsilon_{M0,}$ respectively (Eqs. (12)–(13)). The former (ϵ_T) replaces the recruitment mechanism by the dendritic cells in Su et al. [22], and the latter (ϵ_{M0}) accounts for the decreased macrophage density after a few days of acute inflammation that can be seen in experiments. The recruitment for T_R cells is dependent on the T-cells at the boundary ($\delta\Omega$) [29], which are thought to boost T_R expression through physical contact, and also on the number of T-cells on the entire grid (Ω). For every T on the boundary elements of the grid ($\sum_{\delta\Omega} T$), a T_R is added to a random boundary element of the grid with probability ζ_{TR}(Eq. (13)). T_R cells are typically recruited when LPS is low, and IFNγ is high.

$$\zeta_{T_R} = \begin{cases} \zeta_T \sum_{\Omega} T & \text{if } \int_{\Omega} IFN\gamma > \epsilon_{T_R} \int_{\Omega} LPS \\ 0 & \text{otherwise} \end{cases} \tag{10}$$

$$\zeta_N = \begin{cases} \zeta_N & \text{if } \int_{\Omega} CM < \epsilon_N \\ 0 & \text{otherwise} \end{cases} \tag{11}$$

$$\zeta_{M_0} = \begin{cases} \zeta_{M_0} & \text{if } \int_{\Omega} LPS > \epsilon_{M_0} \\ 0 & \text{otherwise} \end{cases} \tag{12}$$

$$\zeta_T = \begin{cases} \zeta_T & \text{if } \int_{\Omega} LPS > \epsilon_T \\ 0 & \text{otherwise} \end{cases} \tag{13}$$

The model uses two rules for the interaction among agents. First, DLL4 is turned on with probability p(DLL4 = 1|MA) when a macrophage meets one or more MA (i.e., M_1 or M_2) macrophages on a grid point. For each MA on the same grid point, the DLL4 receptor in its gene-regulatory network will turn on with probability p(DLL4 = 1|MA). The second interaction rule states that if an M_2 macrophage is on the same grid point as an ND, the macrophage will engulf it via phagocytosis with probability $p(\lambda_{ND|M2})$. Every time an ND is eliminated, the M_2 macrophage secretes cytokine (CM), according to $\beta_{CM|MA}$. Since CM only determines the recruitment of neutrophils through the total amount of CM present on the grid (Eq. (11)) and does not interact with other cells, CM is not diffused and only degrades over time according to μCM. Recruitment is implemented as initializing a new agent at a random location on the outermost grid points. This means that for every agent outside the grid (i.e., $M0_0$, $T_{0,}$ and N_0), the corresponding agent will be initialized on the boundary with probabilities ζ_{M0}, $\zeta_{T,}$ or ζ_N, respectively. Our model was implemented in Python 3.6 [30] using a package for ABMs called MESA [31].

Table 3
Parameter values for the agent layer, with all the probabilities per Δt of 60 min and conditional probabilities per the molecule concentration or the number of agents present in the same grid point. All cited values are within biological range unless annotated by *, in which case the values are model-specific estimates.

Parameter	Value	Reference
Boundary distributions		
N_b	5000 cells μl^{-1}	[28]
$M0_b$	400 cells μl^{-1}	[28]
T_b	1600 cells μl^{-1}	[28]
Probability of not moving		
$p*_T$	0.34	[22], Eq. (8)
$p*_N$	0.18	[22], Eq. (8)
$p*ND$	0.97	[22]*, Eq. (8)
$p*_M$	0.65	[22], Eq. (8)
Termination probability		
$p(\mu_{N\to ND})$	5.63×10^{-2}	[22], Eq. (9)
$p(\mu_T)$	1.36×10^{-2}	[22], Eq. (9)
$p(\mu_{M0})$	1.37×10^{-4}	[22], Eq. (9)
$p(\mu_{MA})$	2.91×10^{-3}	[22], Eq. (9)
$p(\mu_{ND})$	2.08×10^{-3}	[22]*, Eq. (9)
$p(\lambda_N\|LPS)$	2.27×10^{-2}	[22]*, Eq. (9)
$p(\delta_N\|CH)$	1.24×10^{-2}	[22]*, Eq. (9)
$p(\lambda_{T\|TR})$	2.06×10^{-2}	[22], Eq. (9)
Recruitment parameters		
ϵT_R	0.45 pg μl^{-1}	Estimate
ϵT	0.2 pg μl^{-1}	Estimate
ϵN	2.0×10^{-4} pg μl^{-1}	Estimate
ϵM_0	20 pg μl^{-1}	Estimate
ζ_T	8.5×10^{-5}	Estimate
ζ_M	1.4×10^{-3}	Estimate
ζ_N	4.0×10^{-3}	Estimate
Interaction parameters		
$p(\lambda_{ND\|M2})$	1.0	Estimate
p(DLL4 = 1|MA)	1.0	Estimate

2.3. Parameter calibration and qualitative validation

At first, we tested the GRN and diffusion models separately to ensure each worked correctly. Next, we combined the two models and fine-tuned the parameters that remained to be estimated (Tables 2 and 3). We did this by evaluating the dynamics of the cells and molecules using experimental data. RvD1 was not part of the conducted experiments in either study. As such, the RvD1-associated parameters (e.g., secretion and degradation) were set in our model such that the RvD1 profile matches the qualitative profile of eosinophils [32] (see Section 2.4).

Lacking accurate data on humans, we used data from two animal studies. We used one dataset to calibrate the model and the other dataset to validate it. Firstly, for calibration, we used canine data by Frangogiannis et al. [33] and adjusted our free parameters to match the global dynamics of inflammation of T-cells and macrophages. Since this study only contained six data points (less than the number of free parameters), the parameters were iteratively tuned manually rather than through a parameter optimization method. Afterward, to validate the calibrated model, we used rodent data by Yang et al. [34], which contained neutrophil data in addition to T-cells and macrophages.

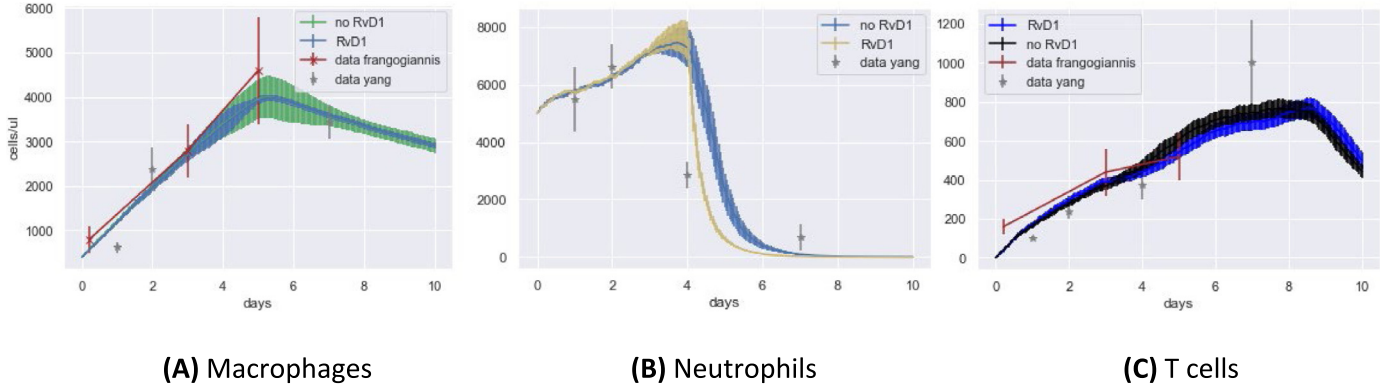

Fig. 3. Temporal dynamics of (A) all macrophages (cells/μl), (B) all neutrophils (cells/μl), and (C) all T cells (cells/μl) compared to data for simulations with and without RvD1. The data points are extracted from Frangogiannis et al. [33] (used for model calibration) and Yang et al. [34] (used for validation only). The bars are 95% confidence intervals.

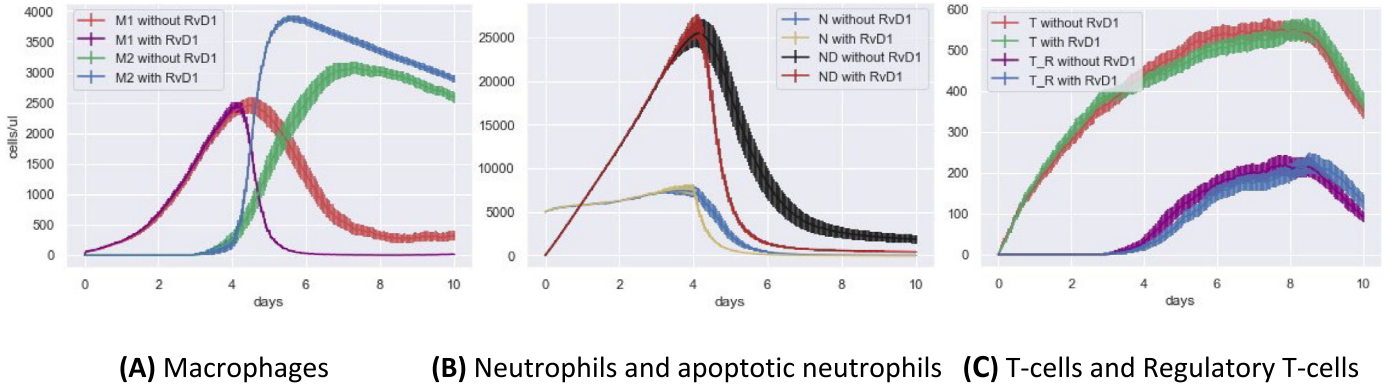

Fig. 4. Temporal dynamics of (A) M_1 and M_2 macrophages (cells/μl), (B) N and ND (cells/μl), and (C) T and T_R (cells/μl) for simulations with and without RvD1. The bars are 95% confidence intervals.

Finally, we conducted a global sensitivity analysis to determine the model's behavior based on the free parameters. The results from this analysis are provided in Appendix D.

The experimental data from these studies were obtained as follows. Except for the exact values specified in the articles, all values were carefully extracted manually from the figures. We assumed that the experimental conditions in the model and the lab experiment were comparable. In particular, we assumed that the data, reported in cells mm^{-2} in both papers, has the same depth as our grid, i.e., 50 μm. We also assumed that the error bars in both publications reported the standard error of the mean specified in Yang et al. [34] but not in Frangogiannis et al. [33]. Also, the data by Yang et al. [34] was re-scaled to match our simulation results (which were fitted to the canine data) since the experiments were performed on mice. Mice have a different immune-cell distribution than humans, while dogs are more similar [35]. The scaling factors were identified by maximizing the error bar overlap to our simulation results by visual inspection and set to 0.3125, 0.5714, and 0.0625 for the macrophages, neutrophils, and T-cells, respectively.

2.4. In silico experiment

We simulated the acute immune response with and without the presence of RvD1. We performed N = 75 runs for each scenario to obtain summary statistics. In these two scenarios, 8 pg of LPS (160 pg μl^{-1}) was injected into the center of the simulated volume at t_0. In the scenario with RvD1 administration, we made several assumptions. RvD1 is the metabolic product of omega 3 PUFAs, which may be secreted by different cell types, like eosinophils, which we do not model explicitly. Since eosinophils get into action when neutrophil count peaks [32] at approximately four days, RvD1 is secreted from that point onwards. RvD1 is secreted from 10% randomly selected grid points, after which it diffuses. RvD1 continues to be secreted until 10 pm μl^{-1} (the experimental value) is reached within approximately four days (i.e., eight days after the start of the simulation), after which the production of RvD1 stops.

To quantify the differences between simulations that included RvD1 and those that did not, we defined an output metric to characterize the behavior of the macrophages. $M_2 > M_1$ is defined as the last moment in time (days) when the density of M_2 becomes greater than M_1 macrophages and stays greater for more than 5 hours straight. We chose this metric because we are more interested in the resolution of inflammation caused by macrophage polarization, and it is more informative than, for instance, the ratio of densities (M_2/M_1).

3. Results

The simulated dynamics of the cells and molecules are shown in Figs. 3–5, reporting cell counts and molecular concentrations on the grid as a function of time. As expected, RvD1 triggers a different behavior in the macrophage differentiation fate, neutrophils dynamics, and CM concentrations (this is the only cytokine profile that appeared to differ in the two scenarios). Fig. 3a and c compare the total number of macrophages and T-cells against experimental data from Frangogiannis et al. [33] and Yang et al. [34]. Moreover, Fig. 3b compares the total number of non-apoptotic neutrophils to data from Yang et al. [34]. Fig. 4 shows the dynamics of the specific cell types, namely M_1 and M_2 macrophages, neutrophils and apoptotic neutrophils, and T cells and regulatory T cells. As can be seen, the neutrophils and macrophages are most affected by the presence of RvD1. In particular, fewer neutrophils

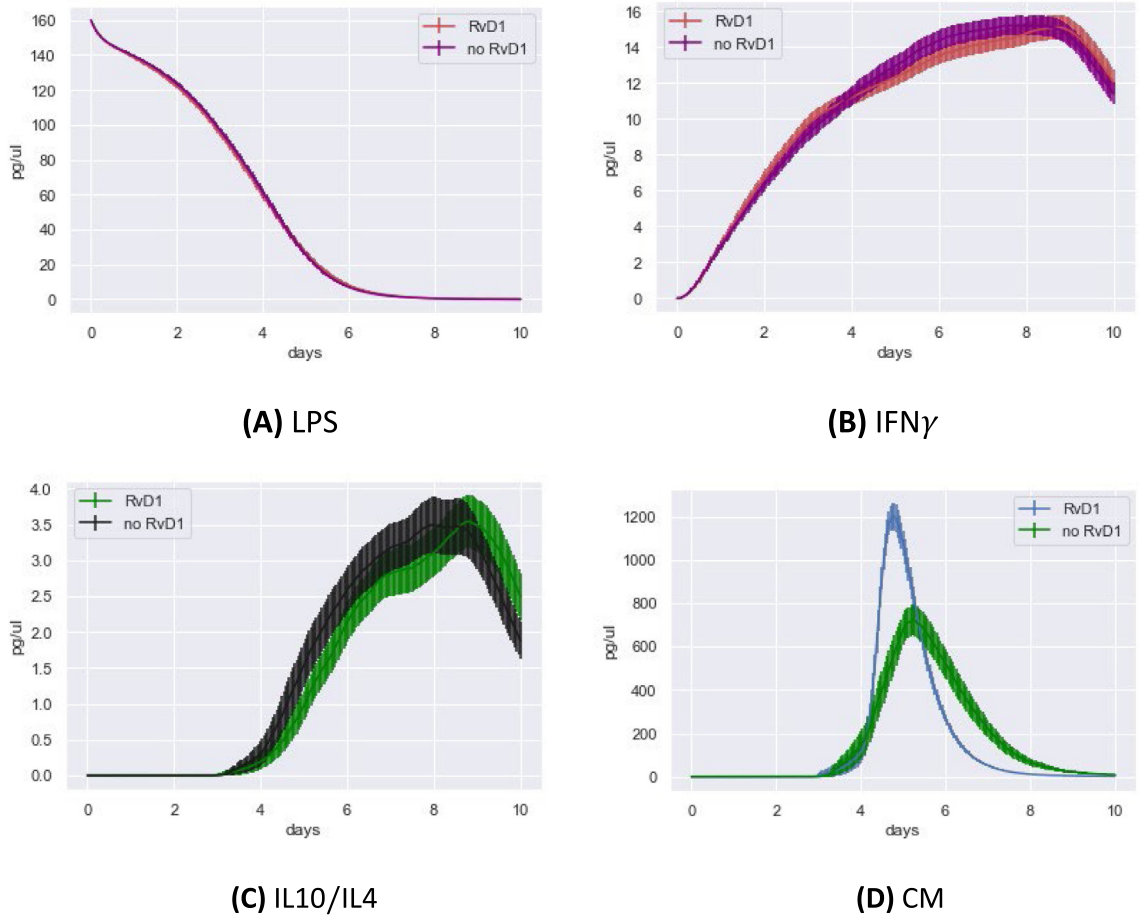

Fig. 5. Plots with temporal dynamics of the total concentrations of (A) LPS, (B) IFNγ, (C) IL10/IL4, and (D) CM (pg/µl) for simulations with and without RvD1. The bars are 95% confidence intervals. CM = cytokine.

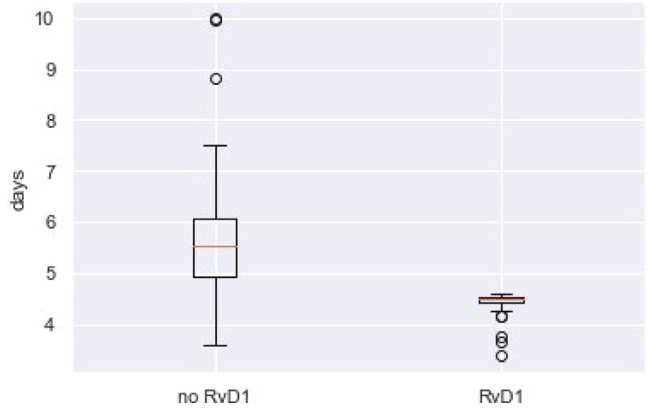

Fig. 6. Boxplot with $M_2 > M_1$ for the simulations with and without RvD1.

are recruited, and apoptotic neutrophils are cleared faster than the control. Furthermore, Fig. 6 shows that when RvD1 is added, $M_2 > M_1$ occurs sooner (after 4.5 days instead of 5.4 days on average) and with much lower variation between the simulations.

4. Discussion

In this paper, we introduced a multiscale hybrid model for acute inflammation to describe the role of RvD1 on macrophage polarization during acute inflammation. It includes a comprehensive GRN model that describes the intracellular mechanisms driving macrophage polarization. The model reproduced the qualitative dynamics of crucial immune cells and the effect of RvD1 during acute inflammation. Our results suggest that RvD1 can drive M_2 macrophage polarization towards an M_2 state faster, reduces neutrophil recruitment, and results in faster apoptotic neutrophil clearance.

Our results agree with several previous modeling studies, including the work by Su et al. [22], on which our model was based. In particular, macrophages in their model peak at about five to six days and T-cells around eight days, which agrees with our results in Fig. 3a and c. However, the neutrophils peak slightly earlier than in our model at about two to three days, which the difference in CM secretion can explain. An important finding from our model, which we could not verify with any experimental data, is $M_2 > M_1$. This happens at around six days in the model by Wang et al. [36]. Our results match this finding well when RvD1 is not added. Moreover, when RvD1 is added, M_2 polarization takes over faster, which is to be expected [37].

We also compared our model to experimental data based on animal models. In particular, we compared our results to historical time-series data of animal models, including the reperfused myocardium in dogs [33], which was also used to calibrate the model. The total number of macrophages and T-cells was compared to Frangogiannis et al. [33] in Fig. 3a and 3c, in which only the first data point of the T-cell results does not match our results because our simulations are initialized without any T-cells present in the tissue. Additionally, Fig. 3 shows the (re-scaled) data points of rodents Yang et al. [34]. The data by Yang et al. [34] were not used to calibrate the model but still qualitatively matched our results well, even for the neutrophils (Fig. 3b), which were not present in the data by Frangogiannis

et al. [33]. Together, these figures suggest that the model captures the global qualitative dynamics of the acute immune response. The initial macrophage recruitment starts earlier in our simulations compared to Yang et al. [34] and agrees with Frangogiannis et al. [33], which is more reliable as it involves a dog model, which is more physiologically relevant to humans than rodents [35]. Also, neutrophils in our model peak slightly later and decline more rapidly. This suggests that a more elaborate recruitment scheme might be needed than the all-or-nothing recruitment (Eq. (11)) or that the neutrophil degradation rate should be lower.

Simulation results of RvD1 administration also agree with other studies. This includes the study by Wang et al. [38], who found that administering 100 ng of RvD1 to mice 30 min before inducing acute lung injury with LPS reduced lung damage. Specifically, Wang et al. [38] found that RvD1 decreased neutrophil recruitment while stimulating neutrophil apoptosis and the expression of IL10. These findings are further supported by Hsiao et al. [37], who also noted an increase in phagocytosis of apoptotic neutrophils and polarization of macrophages to M_2 after RvD1 intake. Our simulation results are in good agreement with these experiments.

Limitations of the model include the lack of human data for calibration and validation of the model and the limited availability of experimental data in animals. Furthermore, several modeled mechanisms may not be realistic. For instance, the absence of IL10 early on in the simulation is unrealistic as a concentration of 0.6 pg μl^{-1} IL10 could already be found after about 24 h of inflammation [39]. Frangogiannis et al. [33] also showed that IL10 levels increase within a few hours after the onset of inflammation. This means that T_R cells should appear sooner in the model, or another type of cell should be secreting IL10 in our model, such as the macrophages or dendritic cells. Generally, T_R cells can take several days to be expressed after infection and, depending on the tissue, take about seven days to peak [40], which agrees with our findings. Therefore, it is more likely that other immune cells need to secrete IL10 to get the correct cytokine profiles. This is important because anti-inflammatory cytokines (secreted by cells other than T_R) early in the simulations could affect the macrophage dynamics in our model.

Another limitation is that the kinetics of the molecules in our model have been validated to a lesser extent than the cells. Lacking more detailed information, we used the same parameter values as Su et al. [22], even though we specify the type of cytokine secreted by T and T_R cells in more detail so that they can function in the GRN model. Nevertheless, these values may be a reasonable approximation. For example, IFNγ secretion by CD4+ T-cells ranged to 50 pg μl^{-1} in stimulated human control tissue [41]. This agrees with our IFNγ values in Fig. 5b. Also, the values of IL10 in Fig. 5c fall within the range of IL10 serum levels in dogs, which range from 31 to 2630 pg.μl^{-1} [42]. Nonetheless, additional evidence is needed to assess whether these modeled cytokines behave as they do in vivo.

Avenues for future work are suggested by the parametric sensitivity analysis (Appendix D), which found that the recruitment probability of T-cells (ζ_T), the activation threshold of RvD1 (θ_{RvD1}), and the recruitment threshold of regulatory T-cells (ϵ_{TR}) had the most significant impact on the moment that M_2 polarized macrophages overtake M_1 ($M_2 > M_1$), resulting in the resolution of acute inflammation. This makes sense because ϵ_{TR} dictates when T_R cells are recruited, being the only cells to secrete anti-inflammatory cytokines in our model. Furthermore, ζ_T determines how many T-cells are recruited, resulting in more and differently distributed cytokines. Finally, RvD1 has a very strong anti-inflammatory effect in the GRN model, so if its threshold (θ_{RvD1}) is lower, RvD1 will steer macrophage polarization towards M_2. Obtaining accurate estimates for these three parameters could be an important focus for experimental research that aims to improve and validate the understanding of the role of RvD1 in macrophage polarization.

Furthermore, extensions of our model could aim to expand on the mechanisms described by these parameters. One improvement could be in the recruitment limit threshold of T (ϵ_T), which is currently dependent on the total LPS concentration in the system. This may be realistic for macrophages, which can be recruited by pathogens [43], but is likely overly simplistic for T-cells. Although our results in Fig. 3a and c indicate that ϵ_M and ϵ_T sufficiently explain the experimental data, these limits are artificial values that, at least for ϵ_T, cannot be easily translated into an actual biological mechanism. Given the sensitivity of our results to ϵ_T, an additional mechanism could be added in the future. For instance, T_R cells might inhibit the recruitment of T-cells, and consequently their own, which they indeed appear to do via IL10 secretion [44]. Furthermore, T_R cells might be recruited by M_2 cells [23]. Implementing such a mechanism into future versions of our model could result in a more realistic description of acute inflammation and, consequently, the mechanistic underpinnings of the effect of SPMs.

Finally, it is recommended that future studies include biological targets not present in our model. The PUFA metabolite RvD1 and other derivatives have been shown to modulate ion channels, such as TRPV1 and TRPA1, which are involved in peripheral nociception and inflammation [45]. Incorporating the effects of PUFA derivatives on various cardiac ion channels [46] and other targets in an extended model may help resolve conflicting clinical data. Those effects include but are not limited to antiarrhythmic activation of potassium channels [47] and inhibition of NHE-1 activity [48]. Moreover, our model can be employed in future simulations to assess the effects of NF-kB inhibitors (e.g., resveratrol and metformin) and JAK/STAT inhibitors (e.g., ruxolitinib and tofacitinib) [49].

5. Conclusion

We developed a multiscale model of an acute inflammatory response and its resolution that integrates two spatial scales of biological organization, intracellular gene regulation, and cell-to-cell interactions at a tissue level. In addition to this integration, we add to previous modeling efforts a combined partial differential equation–agent-based modeling approach, which stochastically describes macrophage activation and M_1 to M_2 polarization.

We applied the model by investigating an SPM of recent interest: RvD1. The model allowed us to run a preliminary in silico experiment to assess the dynamic effect of RvD1 on macrophage polarization. The results from these in silico experiments support a body of literature in which dietary supplementation of SPMs emerges as a feasible and effective candidate in acute and chronic inflammatory disease prevention. Moreover, the model could identify parameters of interest that should be further explored in experimental studies or expanded on in future modeling efforts. This is especially important given the apparent SPM-specific outcomes in clinical trials.

Given that many other in silico experiments are possible, the model could be used as an adaptable framework for studying the effect of various SPMs on acute inflammation, which can become increasingly realistic. Once calibrated and validated on human data, future variants of the model could potentially guide experiments by synthesizing obtained knowledge and identifying critical sources of uncertainty that require further elucidation. This scientific cycle might ultimately result in a deeper understanding of the role of SPMs in macrophage polarization and, hopefully, contribute to developing non-invasive treatments for patients suffering from inflammation-related ailments.

CRediT authorship contribution statement

Jeroen F. Uleman: Conceptualization, Methodology, Software, Writing – original draft. **Emiliano Mancini:** Conceptualization, Supervision, Writing – review & editing. **Rushd F.M. Al-Shama:** Writing – review & editing. **Anje A. te Velde:** Conceptualization, Writing – review & editing. **Aletta D. Kraneveld:** Conceptualization, Writing – review & editing. **Filippo Castiglione:** Conceptualization, Supervision, Writing – review & editing.

Declaration of competing interest

The authors declare that they have no known competing financial interests or personal relationships that could have appeared to influence the work reported in this paper.

Data availability

The code utilized for this study can be obtained upon reasonable request from the first author. The data used to calibrate and validate the model can be found in the referenced literature studies.

Acknowledgments

The authors acknowledge Ksenia Dilevskaya's work on the literature review that was used to extend the gene-regulatory network model. FC acknowledges partial support from the Institute for Advanced Study (IAS), Universiteit van Amsterdam, The Netherlands. The authors also acknowledge Peter M.A. Sloot for supporting this work at the IAS.

Appendix A. Computational methods for modeling inflammation

In systems biology, genetic regulatory networks are used to assemble knowledge of intracellular mechanisms. They include regulators such as DNA, RNA, proteins, and their interactions. However, since it is often impossible to measure all these molecular quantities through wet-lab experiments, reverse engineering biochemical interactions and dynamics through computational modeling is often vital [50]. A distinction can be made between models where the regulators' state takes on a discrete value and continuous models that describe continuous nodes [51]. Although continuous models contain greater detail, discreteness can often be desirable because it enables to use of qualitative data when real-valued data are lacking [51]. Hence, qualitative information about interactions between entities can suffice to develop these models [52].

Computational models have been applied to many biological regulatory systems [53–55]. The simplest among these models is the Boolean network. Network models consist of nodes and edges representing critical regulators of intracellular signaling pathways and their relations. The nodes take values corresponding to activation levels based on the activation of subsets of all other nodes. In the Boolean network case, two activation levels are used: high activity of a particular node and low or absent activity [51]. Network models are typically initialized with a configuration for each node, updated according to specific logical rules at each time step [53]. These updates are based on the activation values of all connected nodes and connections between these nodes. This time evolution of the state of the network can be used as a basis for developing more comprehensive computational models [53].

One such model is the agent-based model (ABM), which discretizes space and time, and uses several rules to describe how the agents interact with an environment. There are several benefits of using the ABM paradigm to represent biological systems. Firstly, ABMs incorporate space, allowing the model dynamics to be driven by local interactions between agents [56]. Agents in the model are also processed in parallel, which allows relatively simple rules on the level of individual agents to result in complex behavior at the global level [56]. Furthermore, ABMs are often stochastic, which is in line with the randomness observed in the behavior of many biological systems [56]. Finally, AMBs have a modular structure, which allows the modeler to easily add new information by changing the agent definition or the interaction rules [56].

Another approach to modeling inflammation is via differential equations, which deterministically describe how one or more quantities change over time. Ordinary differential equations (ODEs) have been used to describe acute inflammation, successfully capturing important qualitative features of macrophage differentiation [36,57]. However, ODEs assume a spatially homogeneous system [58], making them less applicable to situations where spatial effects are important [59]. Partial differential equations (PDEs) explicitly include a spatial component, allowing for spatial heterogeneity [60]. PDEs have also been used to describe macrophage differentiation [22,61]. However, a differential equation approach typically lacks stochasticity, which may not be a realistic way of describing natural systems (although note that deterministic approaches are also often adequate, e.g., in modeling seemingly chaotic behaviors [62]). One way of addressing this shortcoming is to use stochastic differential equations [52]. An alternative approach is hybrid ABM-PDE modeling, an emerging paradigm that is both stochastic and spatially heterogeneous [63–65].

Appendix B. Gene-regulatory network extension

Our gene-regulatory network model (GRN) is an extension of the GRN by Castiglione et al. [20]. The resulting GRN has eight input nodes to sense extracellular stimuli such as cytokines or ligands. These nodes are connected to the corresponding receptors. In addition to the network by Castiglione et al. (2016), our GRN has the Resolvin D1 (RvD1) input signal and corresponding receptor, which is an SPM derived from PUFAs [66]. Furthermore, a DLL4 pathway was added to handle the effects of Notch signaling [67]. Both networks contain inputs and receptors for LPS and cytokines IFNγ, IL10, and IL4. In terms of genes, only Gsk3b has been added. Both models contain iNOS and Arg1, genes that drive polarization between M_1 and M_2 macrophages. Both models also contain pro-inflammation-associated genes STAT1 and NFkB, anti-inflammation-associated genes STAT3, PPARg, KLF4, and STAT6, and genes SOCS3 and SOCS1 that connect them.

Below we provided the additional edges with a corresponding reference to peer-review literature. In particular, we added the Delta-like ligand 4 and Resolvin D1 input signals and corresponding receptors. Additionally, GSK3ß was added as a mediator that affects STAT3.

Delta like ligand 4 (DLL4)
Receptor: Notch1

- (Excitation) Notch1 → NFkB [68]
- (Excitation) Notch1 → STAT1 [69]
- (Excitation) Notch1 → SOCS3 [70]

Resolvin D1 (RvD1)
Receptor: G protein-coupled receptor 32 (GPR32)

- (Inhibition) GPR32 → GSK3ß [71]
- (Inhibition) GPR32 → STAT1 [72]
- (Inhibition) GPR32 → NFkB [73]
- (Excitation) GPR32 → STAT6 [74]

Lipopolysaccharide (LPS)
Receptor: Toll-like receptor 4 (TLR4)

- (Excitation) TLR4 → GSK3ß [75]
- (Excitation) TLR4 → Notch1 [76]

Glycogen synthase kappa B (GSK3ß)

- (Excitation) GSK3ß→ STAT3 [77]

Appendix C. Finite volume method

The Finite Volume Method (FVM), as implemented in the FiPy package, is a subset of the Finite Element Method (FEM) and divides the solution domain into discrete finite volumes over which the state variables are approximated with linear or higher-order interpolations.

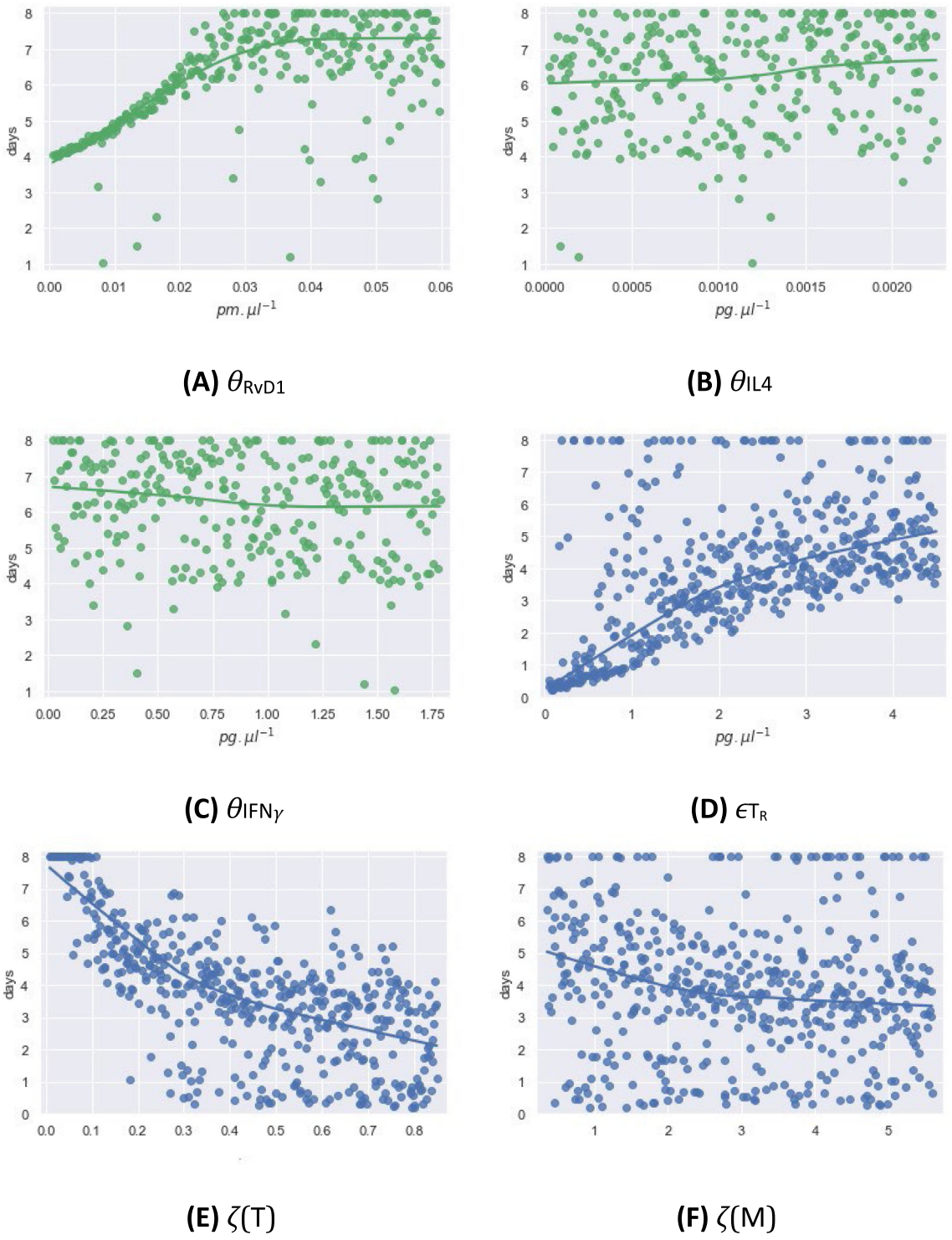

Fig. D.1. Example of global sensitivity analysis for simulations without RvD1 in blue ($N = 500$) and with RvD1 in green (N = 300) with $M_2 > M_1$ as a function of threshold parameters θ_{RvD1},θ_{IL4}, and θ_{IFN_γ} for simulations with RvD1, and ϵ_{TR}, ζ(M) and ζ(T) for simulations without RvD1. The rank correlation coefficients and corresponding p-values for each of the plotted parameters are (A) θ_{RvD1} with $\rho = 0.65$, p = 4.11×10^{-37}, (B) θ_{IL4} with $\rho = 0.17$, p = 2.75×10^{-3}, (C) θ_{IFN_γ} with $\rho = -0.17$, p = 2.75×10^{-3}, (D) ϵ_{TR} with $\rho = 0.58$, p = 8.01×10^{-46}, (E) ζ(T) with $\rho = -0.71$, p = 1.01×10^{-76}, (F) ζ(M) with $\rho = -0.17$, p = 1.65×10^{-4}.

The derivatives in each term of the equation are satisfied with simple approximate interpolations in a process known as discretization [78]. More specifically, FiPy uses Cell Centered (CC)-FVM, in which every control volume (CV) defined by the cells has an average value stored. Cells on the FiPy mesh correspond to grid points in the ABM and are mapped back and forth at every Δt. The CC-FVM method on a Cartesian mesh with cells, faces, and vertices works according to Demirdzic [79]. The face is the divider between two cells for all dimensions. The diffusion equations are approximated by Eq. (14), where ϕ is the solution variable, A_f is the area of face f, and d_{AP} is the distance between neighboring cell centers A and P. The first step transforms the integral over the CV volume (V) into an integral over the CV surface

(S) using the divergence theorem [78].

$$\int_{\mathrm{V}} \nabla \cdot (\mathrm{D}_{\phi} \nabla \phi)\, \mathrm{dV} = \int_{\mathrm{S}} D_{\phi} \left(\vec{n} \cdot \nabla \phi\right) \mathrm{dS} \approx \sum_{\mathrm{f}} \mathrm{D}_{\phi} \left(\vec{n} \cdot \nabla \phi\right)_{\mathrm{f}} \mathrm{A}_{\mathrm{f}} \approx \sum_{f} D_{\phi} \frac{\phi_A - \phi_P}{d_{AP}} A_f \tag{14}$$

The solution to these PDEs can be approximated through several methods. For this particular problem, a Finite Volume PDE Solver package (FiPy) [78] for Python [30] was used. While the straightforward implementation of an explicit numerical scheme to solve the PDEs is generally recommended [21], an implicit scheme is used in our model because it allows for large time steps. In principle, an implicit approach allows for finding direct steady-state solutions to the above equations. We are, however, interested in the intermediate time steps synchronized with the length of the time steps in the ABM (Δt).

Appendix D. Sensitivity analysis

In order to determine the sensitivity of the free parameters in our model, a global sensitivity analysis was performed. The parameter space was sampled using the Latin hypercube method, which was selected for its efficiency compared to completely random sampling methods [80]. Sensitivity analyses were performed for simulations with (N = 300) and without (N = 500) RvD1 in the system.

In the simulations with RvD1, the free parameters that were varied are θ_{LPS}, $\theta_{\mathrm{IFN}_\gamma}$, θ_{IL10}, θ_{IL4}, θ_{RvD1}, $p(_{\mathrm{DLL4=1|MA}})$, $p(\lambda_{\mathrm{ND|M2}})$, ϵ_{TR}, ζ_{M}, and ζ_{T}. In the simulations without RvD1, the same parameters were varied except for RvD1, which was irrelevant. For each free parameter, a range of values was selected, one order of magnitude above and below the values used in our simulations, which for the thresholds and ϵ_{TR} is 0.05 times the reported values in Table 3. The only exceptions were $p(\lambda_{\mathrm{ND|M2}})$ and $p(_{\mathrm{DLL4=1|MA}})$, which ranged between 0.1 and 1.0, and ζ_{M}, which ranged between 50% below and above the used value. The selected ranges were then subdivided into N intervals, each sampled using a uniform distribution. This array of N values was then shuffled randomly and placed inside a matrix with the arrays for the remaining free parameters, giving us a total of N samples from the whole parameter space. Finally, simulations were run using these sets of parameters, after which an output metric, $\mathrm{M}_2 > \mathrm{M}_1$, was calculated and compared between parameter sets.

With $\mathrm{M}_2 > \mathrm{M}_1$ used as an outcome measure, a non-parametric Spearman's ρ rank correlation coefficient was computed for each free parameter and model output. The rank correlation coefficient measures the strength of monotonic associations [81]. Similar approaches were used by Teodoro et al. [82] and Bankhead et al. [83]. Furthermore, a random balance design Fourier Amplitude Sensitivity Test (RBD-FAST), with inference parameter M = 10 harmonics summed in the Fourier series decomposition, was used to calculate first-order sensitivity indices [84]. The RBD-FAST method with Latin hypercube sampling was selected for its computational efficiency and reduced error compared to FAST with random sampling [85]. These first-order sensitivity indices are informative as they yield the exact fraction of the output variance accounted for by any input parameter [86]. Therefore, ideally, rank correlation and variance decomposition are both calculated [87]. Time-varying sensitivity indices could not be calculated because $\mathrm{M}_2 > \mathrm{M}_1$ yields only a single value per simulation.

Some of the sensitivity analysis results can be found in Fig. D.1, where $\mathrm{M}_2 > \mathrm{M}_1$ is plotted for several free parameters for which the rank correlation coefficient had a p-value lower than 0.05. A locally weighted least-squares regression line is drawn in each plot to indicate monotonic trends in the data. The non-parametric Spearman's ρ rank correlation coefficients for the plotted parameters are reported in the caption. Except for ϵ_{TR} in the simulations with RvD1, for which we found $\rho = 0.33$ with a $p = 4.81 \times 10^{-9}$, none of the parameters not plotted in Fig. D.1 correlated significantly to the output. These results are supported by the first-order sensitivity indices (S_i) calculated with the RBD-FAST method. The ranking of the most important effects is almost entirely preserved between the two methods. In simulations without RvD1, we find S_i values of 0.596 for ζ(T), 0.307 for ϵ_{TR}, 0.028 for ζ(M), and 0.014 for θ_{IL4}. The other S_i values are even smaller. In simulations with RvD1, we find S_i values of 0.537 for θ_{RvD1}, 0.247 for ϵ_{TR}, 0.072 for θ_{IL4}, 0.024 for $p(_{\mathrm{DLL4=1|MA}})$, and a very small S_i for IFNγ and the other parameters.

References

[1] J.M. Mullington, N.S. Simpson, H.K. Meier-Ewert, M. Haack, Sleep loss and inflammation, Best Pract. Res. Clin. Endocrinol. Metab. 24 (2010) 775–784.

[2] K.M. Beavers, T.E. Brinkley, B.J. Nicklas, Effect of exercise training on chronic inflammation, Clin. Chim. Acta 411 (2010) 785–793.

[3] K.M. Beavers, B.J. Nicklas, Effects of lifestyle interventions on inflammatory markers in the metabolic syndrome, Front. Biosci. (Sch. Ed.) 3 (2011) 168.

[4] H. Jiang, L. Wang, D. Wang, N. Yan, C. Li, M. Wu, et al., Omega-3 polyunsaturated fatty acid biomarkers and risk of type 2 diabetes, cardiovascular disease, cancer, and mortality, Clin. Nutr. 41 (2022) 1798–1807.

[5] A.A. Bernasconi, M.M. Wiest, C.J. Lavie, R.V. Milani, J.A. Laukkanen, Effect of omega-3 dosage on cardiovascular outcomes: an updated meta-analysis and meta-regression of interventional trials, Mayo Clin. Proc. 96 (2021) 304–313, Elsevier.

[6] F. Kumar, P.K. Tyagi, N.A. Mir, K. Dev, J. Begum, A. Biswas, et al., Dietary flaxseed and turmeric is a novel strategy to enrich chicken meat with long chain ω-3 polyunsaturated fatty acids with better oxidative stability and functional properties, Food Chem. 305 (2020) 125458.

[7] E. Molaei, A. Molaei, A.W. Hayes, G. Karimi, Resolvin D1, therapeutic target in acute respiratory distress syndrome, Eur. J. Pharmacol. 911 (2021) 174527.

[8] G.V. Halade, V. Kain, C.N. Serhan, Immune responsive resolvin D1 programs myocardial infarction–induced cardiorenal syndrome in heart failure, FASEB J. 32 (2018) 3717.

[9] M. Wang, M. Liu, J. Zhang, J. Liu, J. Ye, Y. Xu, et al., Resolvin D1 protects against sepsis-induced cardiac injury in mice, Biofactors 46 (2020) 766–776.

[10] B. Li, B.-C. Yao, Z.-G. Guo, S.-P. Zhang, Y.-Q. Song, N. Jiang, et al., Mechanism of action of resolvin D1 in inhibiting the progression of aortic dissection in mice, Ann. Transl. Med. 9 (2021).

[11] M. Ponzoni, F. Pastorino, D. Di Paolo, P. Perri, C. Brignole, Targeting macrophages as a potential therapeutic intervention: Impact on inflammatory diseases and cancer, Int. J. Mol. Sci. 19 (2018).

[12] Y. Oishi, I. Manabe, Macrophages in age-related chronic inflammatory diseases, NPJ Aging Mech. Dis. 2 (2016) 1–8.

[13] C.N. Serhan, Pro-resolving lipid mediators are leads for resolution physiology, Nature 510 (2014) 92–101.

[14] G. Curfman, Omega-3 fatty acids and atrial fibrillation, JAMA 325 (2021) 1063.

[15] P.L. Myhre, A.A. Kalstad, S.H. Tveit, K. Laake, E.B. Schmidt, P. Smith, et al., Changes in eicosapentaenoic acid and docosahexaenoic acid and risk of cardiovascular events and atrial fibrillation: A secondary analysis of the OMEMI trial, J. Internal Med. 291 (2022) 637–647.

[16] S. Motta, F. Pappalardo, Mathematical modeling of biological systems, Brief. Bioinform. 14 (2013) 411–422, http://dx.doi.org/10.1093/bib/bbs061.

[17] Z. Wang, J.D. Butner, R. Kerketta, V. Cristini, T.S. Deisboeck, Simulating cancer growth with multiscale agent-based modeling, in: Seminars in Cancer Biology, Vol. 30, Elsevier, 2015, pp. 70–78.

[18] H. de Jong, Modeling and simulation of genetic regulatory systems: A literature review, J. Comput. Biol. 9 (2002) 67–103, http://dx.doi.org/10.1089/10665270252833208.

[19] A. Cappuccio, P. Tieri, F. Castiglione, Multiscale modelling in immunology: a review, Brief. Bioinform. 17 (2015) 408–418.

[20] F. Castiglione, P. Tieri, A. Palma, A.S. Jarrah, Statistical ensemble of gene regulatory networks of macrophage differentiation, BMC Bioinformatics 17 (2016) http://dx.doi.org/10.1186/s12859-016-1363-4.

[21] N. Cilfone, D. Kirschner, J. Linderman, Strategies for efficient numerical implementation of hybrid multi-scale agent-based models to describe biological systems, Cell. Mol. Bioeng. 8 (2015) 119–136, http://dx.doi.org/10.1016/S2214-109X(16)30265-0, Cost-effectiveness.

[22] B. Su, W. Zhou, K.S. Dorman, D.E. Jones, Mathematical modelling of immune response in tissues, Comput. Math. Methods Med. 10 (2009) 9–38, http://dx.doi.org/10.1080/17486700801982713.

[23] G. Arango Duque, A. Descoteaux, Macrophage cytokines: involvement in immunity and infectious diseases, Front. Immunol. 5 (2014) 491.

[24] T. Palaga, C. Buranaruk, S. Rengpipat, A.H. Fauq, T.E. Golde, S.H. Kaufmann, et al., Notch signaling is activated by TLR stimulation and regulates macrophage functions, Eur. J. Immunol. 38 (2008) 174–183.

[25] M. Santillán, On the use of the Hill functions in mathematical models of gene regulatory networks, Math. Model. Nat. Phenom. 3 (2008) 85–97.

[26] X. Dong, D. Chu, Z. Wang, Leukocyte-mediated delivery of nanotherapeutics in inflammatory and tumor sites, Theranostics 7 (2017) 751.

[27] Z. Tong, E.M. Balzer, M.R. Dallas, W.-C. Hung, K.J. Stebe, K. Konstantopoulos, Chemotaxis of cell populations through confined spaces at single-cell resolution, PLoS One 7 (2012) e29211.

[28] A. Tefferi, C.A. Hanson, D.J. Inwards, How to interpret and pursue an abnormal complete blood cell count in adults, Mayo Clin. Proc. 80 (2005) 923–936, Elsevier.

[29] D.A. Vignali, L.W. Collison, C.J. Workman, How regulatory T cells work, Nat. Rev. Immunol. 8 (2008) 523.

[30] Python Core Team, Python: A Dynamic, Open Source Programming Language, Python Software Foundation, 2015.

[31] ProjectMesa, Mesa documentation, 2018.

[32] Y. Isobe, T. Kato, M. Arita, Emerging roles of eosinophils and eosinophil-derived lipid mediators in the resolution of inflammation, Front. Immunol. 3 (2012) 270.

[33] N.G. Frangogiannis, L.H. Mendoza, M.L. Lindsey, C.M. Ballantyne, L.H. Michael, C.W. Smith, et al., IL-10 is induced in the reperfused myocardium and may modulate the reaction to injury, J. Immunol. 165 (2000) 2798–2808.

[34] F. Yang, Y.-H. Liu, X.-P. Yang, J. Xu, A. Kapke, O.A. Carretero, Myocardial infarction and cardiac remodelling in mice, Exp. Physiol. 87 (2002) 547–555.

[35] P. Felsburg, Overview of immune system development in the dog: comparison with humans, Hum. Exp. Toxicol. 21 (2002) 487–492.

[36] Y. Wang, T. Yang, Y. Ma, G.V. Halade, J. Zhang, M.L. Lindsey, et al., Mathematical modeling and stability analysis of macrophage activation in left ventricular remodeling post-myocardial infarction, BMC Genom. 13 (2011) S21, http://dx.doi.org/10.1186/1471-2164-13-S6-S21.

[37] H.-M. Hsiao, R.E. Sapinoro, T.H. Thatcher, A. Croasdell, E.P. Levy, R.A. Fulton, et al., A novel anti-inflammatory and pro-resolving role for resolvin D1 in acute cigarette smoke-induced lung inflammation, PLoS One 8 (2013) e58258.

[38] L. Wang, R. Yuan, C. Yao, Q. Wu, M. Christelle, W. Xie, et al., Effects of resolvin D1 on inflammatory responses and oxidative stress of lipopolysaccharide-induced acute lung injury in mice, Chin. Med. J. 127 (2014) 803–809.

[39] S.S. Iyer, A.A. Ghaffari, G. Cheng, Lipopolysaccharide-mediated IL-10 transcriptional regulation requires sequential induction of type I IFNs and IL-27 in macrophages, J. Immunol. (2010) 1002041.

[40] J. Li, J. Tan, M.M. Martino, K.O. Lui, Regulatory T-cells: Potential regulator of tissue repair and regeneration, Front. Immunol. 9 (2018) 585.

[41] I.J. Fuss, M. Neurath, M. Boirivant, J.S. Klein, C. De La Motte, S.A. Strong, et al., Disparate CD4+ lamina propria (LP) lymphokine secretion profiles in inflammatory bowel disease. Crohn's disease LP cells manifest increased secretion of IFN-gamma, whereas ulcerative colitis LP cells manifest increased secretion of IL-5, J. Immunol. 157 (1996) 1261–1270.

[42] D.M. Sawyere, O.I. Lanz, L.A. Dahlgren, S.L. Barry, A.C. Nichols, S.R. Werre, Cytokine and growth factor concentrations in canine autologous conditioned serum, Vet. Surg. 45 (2016) 582–586.

[43] C. Shi, E.G. Pamer, Monocyte recruitment during infection and inflammation, Nat. Rev. Immunol. 11 (2011) 762.

[44] X. Zhou, M.S. Fragala, J.E. McElhaney, G.A. Kuchel, Conceptual and methodological issues relevant to cytokine and inflammatory marker measurements in clinical research, Curr. Opin. Clin. Nutr. Metab. Care 13 (2010) 541.

[45] R.-R. Ji, Z.-Z. Xu, G. Strichartz, C.N. Serhan, Emerging roles of resolvins in the resolution of inflammation and pain, Trends Neurosci. 34 (2011) 599–609.

[46] C. Moreno, Á. Macías, Á. Prieto, A. De La Cruz, T. González, C. Valenzuela, Effects of n- 3 polyunsaturated fatty acids on cardiac ion channels, Front. Physiol. 3 (2012) 245.

[47] C. Moreno, A. de La Cruz, A. Oliveras, S.R. Kharche, M. Guizy, N. Comes, et al., Marine n-3 PUFAs modulate I Ks gating, channel expression, and location in membrane microdomains, Cardiovasc. Res. 105 (2015) 223–232.

[48] M.M. van Borren, H.M. Den Ruijter, A. Baartscheer, J.H. Ravesloot, R. Coronel, A.O. Verkerk, Dietary omega-3 polyunsaturated fatty acids suppress NHE-1 upregulation in a rabbit model of volume-and pressure-overload, Front. Physiol. 3 (2012) 76.

[49] A. Soto-Gamez, M. Demaria, Therapeutic interventions for aging: the case of cellular senescence, Drug Discov. Today 22 (2017) 786–795.

[50] O. Angelin-Bonnet, P.J. Biggs, M. Vignes, Gene regulatory networks: a primer in biological processes and statistical modelling, 2018, ArXiv Preprint arXiv:180501098.

[51] G. Karlebach, R. Shamir, Modelling and analysis of gene regulatory networks, Nat. Rev. Mol. Cell Biol. 9 (2008) 770–780, http://dx.doi.org/10.1038/nrm2503.

[52] Y. Vodovotz, A. Xia, E.L. Read, J. Bassaganya-Riera, D.A. Hafler, E. Sontag, et al., Solving immunology? Trends Immunol. 38 (2017) 116–127.

[53] A. Naldi, D. Berenguier, A. Fauré, F. Lopez, D. Thieffry, C. Chaouiya, Logical modelling of regulatory networks with GINsim 2.3, BioSystems 97 (2009) 134–139, http://dx.doi.org/10.1016/j.biosystems.2009.04.008.

[54] C. Espinosa-Soto, P. Padilla-Longoria, E.R. Alvarez-Buylla, A gene regulatory network model for cell-fate determination during arabidopsis thalianal flower development that is robust and recovers experimental gene expression profiles, Plant Cell 16 (2004) 2923–2939, http://dx.doi.org/10.1105/tpc.104.021725.2.

[55] G. Bernot, J.P. Comet, A. Richard, J. Guespin, Application of formal methods to biological regulatory networks: Extending Thomas' asynchronous logical approach with temporal logic, J. Theoret. Biol. 229 (2004) 339–347, http://dx.doi.org/10.1016/j.jtbi.2004.04.003.

[56] G. An, Q. Mi, J. Dutta-Moscato, Y. Vodovotz, Agent-based models in translational systems biology, Wiley Interdiscip. Rev.: Syst. Biol. Med. 1 (2009) 159–171.

[57] R. Kumar, G. Clermont, Y. Vodovotz, C.C. Chow, The dynamics of acute inflammation, J. Theoret. Biol. 230 (2004) 145–155, http://dx.doi.org/10.1016/j.jtbi.2004.04.044.

[58] X. Dong, P.T. Foteinou, S.E. Calvano, S.F. Lowry, I.P. Androulakis, Agent-based modeling of endotoxin-induced acute inflammatory response in human blood leukocytes, PLoS ONE 5 (2010) http://dx.doi.org/10.1371/journal.pone.0009249.

[59] G. An, Introduction of an agent-based multi-scale modular architecture for dynamic knowledge representation of acute inflammation, Theor. Biol. Med. Model. 5 (2008) 1–20, http://dx.doi.org/10.1186/1742-4682-5-11.

[60] Y. Vodovotz, G. Constantine, J. Rubin, M. Csete, E.O. Voit, G. An, Mechanistic simulations of inflammation: Current state and future prospects, Math. Biosci. 217 (2009) 1–10, http://dx.doi.org/10.1016/j.mbs.2008.07.013.

[61] A.B. Pigozzo, G.C. Macedo, R.W. dos Santos, M. Lobosco, Implementation of a computational model of the innate immune system, in: ICARIS, 2011, pp. 95–107.

[62] D. Sato, L.-H. Xie, T.P. Nguyen, J.N. Weiss, Z. Qu, Irregularly appearing early afterdepolarizations in cardiac myocytes: random fluctuations or dynamical chaos? Biophys. J. 99 (2010) 765–773.

[63] M.H. Zangooei, J. Habibi, Hybrid multiscale modeling and prediction of cancer cell behavior, PLOS ONE 12 (2017) 1–26, http://dx.doi.org/10.1371/journal.pone.0183810.

[64] S. Banerjee, M.E. Moses, A hybrid agent based and differential equation model of body size effects on pathogen replication and immune system response, in: International Conference on Artificial Immune Systems, Springer, 2009, pp. 14–18.

[65] L. Caudill, B. Lawson, A hybrid agent-based and differential equations model for simulating antibiotic resistance in a hospital ward, in: Proceedings of the 2013 Winter Simulation Conference: Simulation: Making Decisions in a Complex World, IEEE Press, 2013, pp. 1419–1430.

[66] C.N. Serhan, N.A. Petasis, Resolvins and protectins in inflammation-resolution, Chem. Rev. 10 (2011) 5922–5943.

[67] T. Nakano, D. Fukuda, J. Koga, M. Aikawa, Dll4-notch signaling in macrophage activation, Arterioscler. Thromb. Vasc. Biol. 36 (2016) 2038–2047.

[68] E. Fung, S.-M.T. Tang, J.P. Canner, K. Morishige, J.F. Arboleda-Velasquez, A.A. Cardoso, et al., Delta-like 4 induces notch signaling in macrophages: implications for inflammation, Circulation 115 (2007) 2948–2956.

[69] E. Monsalve, M.A. Pérez, A. Rubio, M.J. Ruiz-Hidalgo, V. Baladrón, J.J. García-Ramírez, et al., Notch-1 up-regulation and signaling following macrophage activation modulates gene expression patterns known to affect antigen-presenting capacity and cytotoxic activity, J. Immunol. 176 (2006) 5362–5373.

[70] Y.-C. Wang, F. He, F. Feng, X.-W. Liu, G.-Y. Dong, H.-Y. Qin, et al., Notch signaling determines the M1 versus M2 polarization of macrophages in antitumor immune responses, Cancer Res. 70 (2010) 4840–4849.

[71] Z. Gu, G.J. Lamont, R.J. Lamont, S.M. Uriarte, H. Wang, D.A. Scott, Resolvin D1, resolvin D2 and maresin 1 activate the GSK3β anti-inflammatory axis in TLR4-engaged human monocytes, Innate Immunity 22 (2016) 186–195.

[72] E. Titos, B. Rius, C. López-Vicario, J. Alcaraz-Quiles, V. García-Alonso, A. Lopategi, et al., Signaling and immunoresolving actions of resolvin D1 in inflamed human visceral adipose tissue, J. Immunol. 197 (2016) 3360–3370, http://dx.doi.org/10.4049/jimmunol.1502522.

[73] A. Recchiuti, S. Krishnamoorthy, G. Fredman, N. Chiang, C.N. Serhan, MicroRNAs in resolution of acute inflammation: identification of novel resolvin D1-miRNA circuits, FASEB J. 25 (2011) 544.

[74] L. Li, Y. Wu, Y. Wang, J. Wu, L. Song, W. Xian, et al., Resolvin D1 promotes the interleukin-4-induced alternative activation in BV-2 microglial cells, J. Neuroinflamm. 11 (2014) 1–11.

[75] X. Hu, P.K. Paik, J. Chen, A. Yarilina, L. Kockeritz, T.T. Lu, et al., IFN-γ suppresses IL-10 production and synergizes with TLR2 by regulating GSK3 and CREB/AP-1 proteins, Immunity 24 (2006) 563–574.

[76] S. Artavanis-Tsakonas, M.D. Rand, R.J. Lake, Notch signaling: cell fate control and signal integration in development, Science 284 (1999) 770–776.

[77] H. Wang, J. Brown, M. Martin, Glycogen synthase kinase 3: a point of convergence for the host inflammatory response, Cytokine 53 (2011) 130–140.

[78] J.E. Guyer, D. W, J.A. W, FiPy: Partial Differential Equations with Python, 2009.

[79] I. Demirdžić, On the discretization of the diffusion term in finite-volume continuum mechanics, Numer. Heat Transfer B 68 (2015) 1–10.
[80] R.L. Iman, J.M. Davenport, D.K. Zeigler, Latin Hypercube Sampling (Program User's Guide).[LHC, in FORTRAN], Sandia Labs., Albuquerque, NM (USA), 1980.
[81] P. Sedgwick, Spearman's rank correlation coefficient, Bmj 349 (2014) g7327.
[82] G. Teodoro, T.M. Kurç, L.F. Taveira, A.C. Melo, Y. Gao, J. Kong, et al., Algorithm sensitivity analysis and parameter tuning for tissue image segmentation pipelines, Bioinformatics 33 (2016) 1064–1072.
[83] A. Bankhead, E. Mancini, A.C. Sims, R.S. Baric, S. McWeeney, P.M. Sloot, A simulation framework to investigate in vitro viral infection dynamics, J. Comput. Sci. 4 (2013) 127–134.
[84] S. Tarantola, D. Gatelli, T.A. Mara, Random balance designs for the estimation of first order global sensitivity indices, Reliab. Eng. Syst. Saf. 91 (2006) 717–727.
[85] C. Xu, G. Gertner, Understanding and comparisons of different sampling approaches for the Fourier Amplitudes Sensitivity Test (FAST), Comput. Statist. Data Anal. 55 (2011) 184–198.
[86] T. Homma, A. Saltelli, Importance measures in global sensitivity analysis of nonlinear models, Reliab. Eng. Syst. Saf. 52 (1996) 1–17.
[87] S. Marino, I.B. Hogue, C.J. Ray, D.E. Kirschner, A methodology for performing global uncertainty and sensitivity analysis in systems biology, J. Theoret. Biol. 254 (2008) 178–196.